Nej1 interacts with Sae2 at DNA double-stranded breaks to inhibit DNA resection

Aditya Mojumdar[ORCID]**, Nancy Adam, and Jennifer A. Cobb***

From the Departments of Biochemistry & Molecular Biology and Oncology, Robson DNA Science Centre, Arnie Charbonneau Cancer Institute, Cumming School of Medicine, University of Calgary, Calgary, Alberta, Canada

Edited by Patrick Sung

The two major pathways of DNA double-strand break repair, nonhomologous end-joining and homologous recombination, are highly conserved from yeast to mammals. The regulation of 5′-DNA resection controls repair pathway choice and influences repair outcomes. Nej1 was first identified as a canonical NHEJ factor involved in stimulating the ligation of broken DNA ends, and more recently, it was shown to participate in DNA end-bridging and in the inhibition of 5′-resection mediated by the nuclease/helicase complex Dna2–Sgs1. Here, we show that Nej1 interacts with Sae2 to impact DSB repair in three ways. First, we show that Nej1 inhibits interaction of Sae2 with the Mre11–Rad50–Xrs2 complex and Sae2 localization to DSBs. Second, we found that Nej1 inhibits Sae2-dependent recruitment of Dna2 independently of Sgs1. Third, we determined that *NEJ1* and *SAE2* showed an epistatic relationship for end-bridging, an event that restrains broken DNA ends and reduces the frequency of genomic deletions from developing at the break site. Finally, we demonstrate that deletion of *NEJ1* suppressed the synthetic lethality of *sae2Δ sgs1Δ* mutants, and that triple mutant viability was dependent on Dna2 nuclease activity. Taken together, these findings provide mechanistic insight to how Nej1 functionality inhibits the initiation of DNA resection, a role that is distinct from its involvement in end-joining repair at DSBs.

DNA double-strand breaks (DSBs) can be repaired by two central pathways, nonhomologous end joining (NHEJ) and homologous recombination (HR). NHEJ mediates the direct ligation of DNA ends without the requirement for end processing, whereas HR requires 5′ end resection. Both 5′ resection and end-bridging are important for repair pathway choice and downstream outcomes. Once resection initiates, repair by canonical NHEJ is no longer an option. This key step is regulated by a network of proteins, including Nej1, which was first identified as a core NHEJ factor (1–9).

yKu70–80 (Ku) and Mre11–Rad50–Xrs2 (MRX) are the first complexes that localize to DSBs and both are important for recruiting Nej1 (1–4). Cells lacking *NEJ1* are as defective in end-joining repair as *ku70Δ* and *dnl4Δ* (3, 5, 6). Moreover, Nej1 also contributes to Ku stability, which protects the DNA ends from nucleolytic degradation, and promotes Lif1-Dnl4–mediated ligation (2, 3, 7, 8). Nej1 also functions in collaboration with MRX to bridge DNA ends at the DSB. The structural features of the MRX complex are critical for end-bridging, and deletion of *NEJ1* results in end-bridging defects that are additive with *rad50* mutants (4, 10–13). While Nej1 and MRX both contribute to DNA end-bridging, Nej1 functions antagonistically to MRX as it inhibits 5′ DNA resection. Currently, few mechanistic details exist for how Nej1 inhibits resection, although previous work showed that Nej1 inhibits Dna2 interactions with Sgs1 and Mre11 (4). As work with Nej1 continues to emerge, it is becoming clear that its role in DSB repair involves more than stimulating Dnl4 ligase and stabilizing Ku during NHEJ.

5′ DNA resection occurs through a two-step process (14). First, Sae2, the yeast homolog of human CtIP, activates Mre11 endonuclease to initiate DNA resection, which also promotes Ku dissociation from the DNA ends (15, 16). Second, long-range resection follows, which is mediated by two functionally redundant 5′ to 3′ nucleases, Dna2, in complex with Sgs1, and Exo1 (16, 17). Mre11 endonuclease activity is less critical for initiating 5′ resection than its physical presence at DSBs because both Exo1 and Dna2-Sgs1 can serve as compensatory back-ups, however both long-range nucleases require MRX for their localization (9, 17, 18). Exo1 has high affinity for DNA ends and can initiate resection in *mre11* nuclease dead (nd) mutants only when *KU70* is deleted (19, 20). By contrast, when *NEJ1* is deleted, Exo1-mediated resection did not occur indicating that a certain level of Ku is maintained at DSBs in *nej1Δ* mutants (4, 9).

Regulation of Dna2-dependent resection seems to be more complex than Exo1, which appears to only require DNA ends not protected by Ku. Furthermore, understanding the function of Dna2 at DSBs has been challenging because *DNA2* is an essential gene involved in Okazaki fragment processing and cannot be deleted (21–25). Earlier work showed that the lethality of *dna2Δ* can be suppressed by disruption of *PIF1* helicase and that the frequency of 5′ resection decreased at a DSB in *dna2Δ pif1*-m2 mutants (19, 26). In the absence of Mre11 nuclease activity, resection initiates primarily through Dna2, independently of *KU* status (27–29). Moreover, using nuclease-deficient *dna2*-1 (P504→S), Dna2 and Mre11 showed functional redundancy for processing the ends of DSBs after

* For correspondence: Jennifer A. Cobb, jcobb@ucalgary.ca.

radiation treatment (30). Most work-describing Dna2 at DSBs has been performed in surrogate, by deleting *SGS1* (16, 31). However, those studies cannot explain the greater IR and UV sensitivity of *dna2*-1 *sgs1Δ* mutants than single mutant counterparts (32) and would not be able to identify any potential function(s) for Dna2 at DSBs independently of Sgs1.

In humans, CtIP was shown to be another pathway for Dna2 recruitment to DSB (33). While this has yet to be demonstrated in yeast with Sae2, recently it was shown that Sae2 stimulates the nuclease and helicase activity of Dna2-Sgs1 *in vitro* (34, 35). Sae2 also has a role in DNA end-bridging at DSBs (36), a function conserved in humans and with Ctp1 in fission yeast (37, 38). As both Nej1 and Sae2 have roles in end-bridging, yet function antagonistically to inhibit and promote resection respectively, investigating their relationship at DSBs is needed.

In the present work, we show that Sae2 at DSBs is a key factor in Dna2 recruitment. Nej1 binds and inhibits Sae2 interactions with each component of the MRX complex and its interaction with Dna2. We also demonstrate that Nej1 functions in opposition to Dna2 and Sae2 in DNA end processing at DSBs. The deletion of *NEJ1* led to increased 5′ resection and Sae2-dependent recovery of Dna2 at the break. We also show that deletion of *NEJ1* can suppress the synthetic lethality (SL) of *sae2Δ sgs1Δ* through a mechanism dependent on the nuclease activity of Dna2. By contrast, epistatic end-bridging defects were seen in cells harboring *NEJ1* and *SAE2* deletions. Thus, distinct from their opposing relationship in regulating 5′ resection, Nej1–Sae2 interactions might restrict the mobility DNA ends at the break, an event important for both NHEJ and HR repair at DSBs.

Results

Nej1 inhibits Sae2 recovery at a DSB

Sae2 initiates DNA end-resection by activating Mre11 endonuclease (16). By contrast, Nej1 interacts with the C-terminus of Mre11 and inhibits resection (4, 9). Because these factors regulate 5′ resection in opposition and both depend on MRX for their localization (4, 28), we were prompted to investigate the interplay between them at the site-specific homothallic (HO)-DSB. First, we performed chromatin immuno-precipitation (ChIP) on Sae2 with primers located 0.6 kb from the DSB (Fig. 1*A*). Consistent with previous work, Sae2 decreased to background levels in *mre11Δ* mutants (Fig. 1*B*). By contrast, Sae2 recovery increased ∼2-fold in *nej1Δ* mutants from 40 min to 3 h after HO induction (Fig. 1, *B* and *C*). This was not an indirect consequence of disrupting NHEJ repair in general because Sae2 did not increase in cells where *KU70* or *DNL4* was deleted (Fig. 1*B*). Next, we assessed the importance of Sae2 in Nej1 localization. No change was seen in Nej1 recovery in *sae2Δ* mutants, which was somewhat surprising given that Ku70 recovery increased in *sae2Δ* mutants (Fig. S1*A*, (19)), and Nej1 recovery in *mre11Δ* was reduced to background (Fig. 1*D*).

To determine whether there was a physical interaction between Nej1 and Sae2, we next performed yeast two-hybrid

(Y2H) as previously described (4, 8). This approach was used because Nej1 has a short half-life, making coimmunoprecipitation methods difficult (4, 5, 8, 39, 40). Sae2 was expressed as hemagglutinin (HA)-tagged prey and Nej1 was expressed as LexA-tagged bait (4, 8, 41). Sae2 showed robust binding with Nej1 upon galactose (GAL) induction independently of Mre11 (Figs. 1*E* and S1*B*). We also performed Y2H between Sae2 and each component of the MRX complex. Consistent with previous reports (42), Sae2 physically interacted with Mre11, Rad50, and Xrs2 when expressed as LexA-tagged bait (light blue bars, Fig. 1*F*), and all interactions increased in *nej1Δ* mutants (dark blue bars, Figs. 1*F* and S1*B*). Western blots showed that constructs expressed similarly in WT and *nej1Δ* backgrounds after GAL induction (Fig. S1, *C* and *D*). Thus, when a DSB occurs, Nej1 could inhibit Sae2 recruitment in two ways. First, through direct binding to Sae2 and secondly, through interacting with MRX as we previously mapped Nej1–MRX interactions to Mre11, which we show here to occur independently of Sae2 (Fig. S1*E*) (4).

Given that Sae2 promotes resection whereas Nej1 inhibits it, we next measured 5′ resection directly at the DSB using a quantitative PCR-based approach developed by others and previously performed by us (4, 9, 36, 43). It relies on an *Rsa*I cut site located 0.15 kb from the DSB (Fig. 1*A*). If resection has proceeded past this site, then ssDNA is produced, and the region can be amplified by PCR using primers that flank the restriction site. Deletion of *SAE2* reversed the elevated rate of 5′ resection in *nej1Δ* mutants (Fig. 1*G*). The increased rate of resection in *nej1Δ* was dependent on a pathway involving Sae2 as double mutants showed reduced resection, which was below WT but above *sae2Δ* mutants. Taken together, our results suggest that Nej1 inhibits Sae2 localization and Sae2-mediated 5′ DNA resection.

Nej1 regulates resection and HR by inhibiting Dna2 and Sae2

When Mre11 nuclease is not activated, as in *sae2Δ* mutants, resection initiates primarily from the activity of Dna2-Sgs1. These findings, together with our previous work showing Nej1 inhibits Dna2-Sgs1 (4), prompted us to determine the level of Dna2 recovery in nuclease-dead *mre11*-3 mutants. The MRX complex is recovered similarly in *MRE11*+ and *mre11*-3 mutants, which is important as both Exo1 and Dna2 nucleases require MRX for their localization (44, 45). Dna2 recovery in *nej1Δ mre11*-3 and *nej1Δ* mutants was ∼2-fold above WT (Fig. 2*A*, (4)). Consistent with this increase, both mutants also showed increased resection (Fig. 2*B*). Increased resection in *nej1Δ mre11*-3 and *nej1Δ* mutants was reversed to WT levels by deleting *SGS1* (Fig. 2, *B* and *D*). Surprisingly, Dna2 recovery remained high in *nej1Δ mre11*-3 *sgs1Δ* triple mutants (Fig. 2*A*). In fact, Dna2 increased in all genetic combinations where *SGS1* was deleted together with *NEJ1* (Fig. 2, *A* and *C*). In *sgs1Δ* single mutants, the recovery level of Dna2 was reduced, however, levels remained well above the nontagged control (Fig. 2*C*). Taken together, these results indicate a pathway for Dna2 recruitment to DSBs that was Sgs1 independent and one that was also inhibited by Nej1. While resection became more
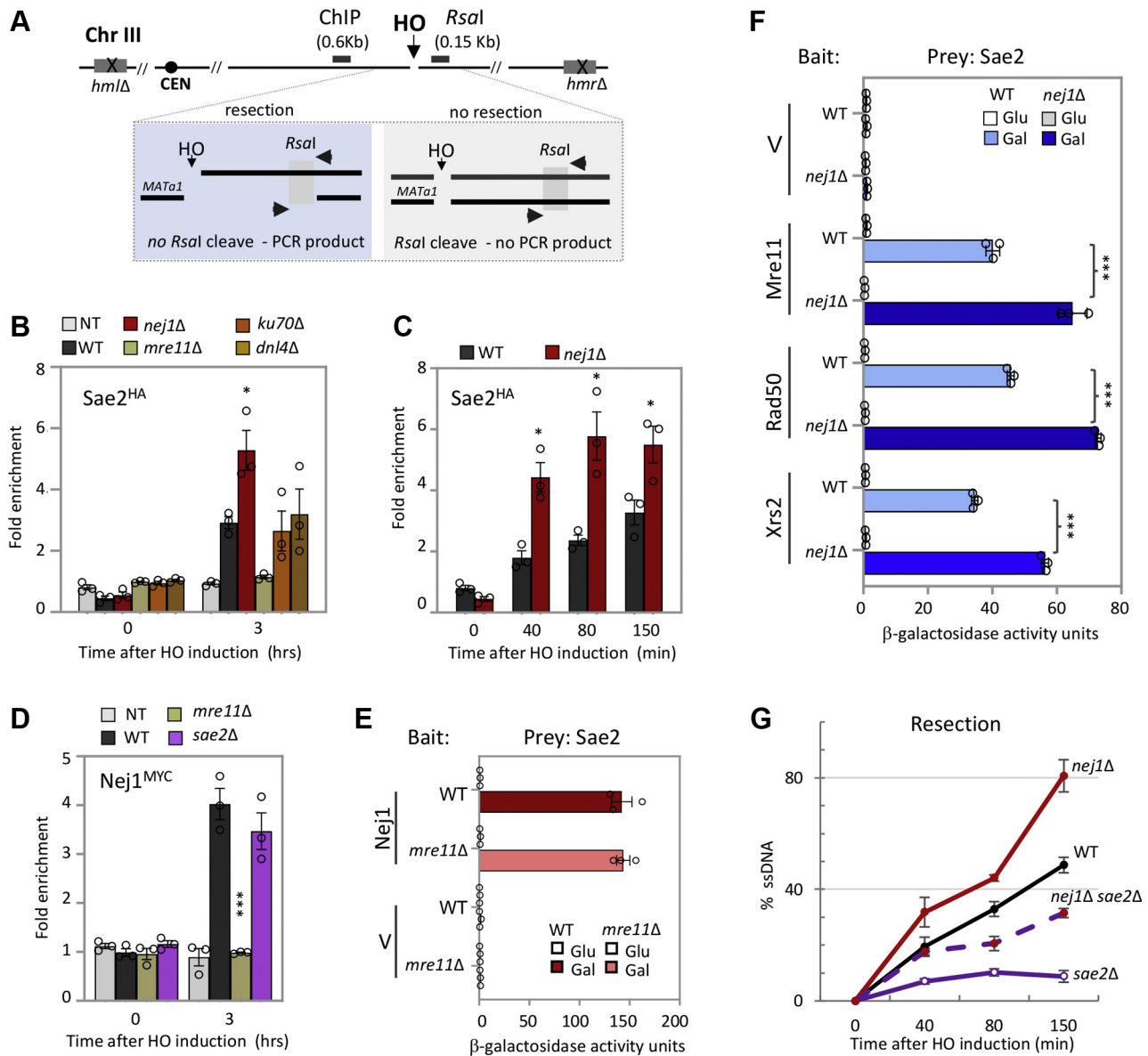
Figure 1. Sae2 recruitment at DSB is inhibited by Nej1. *A*, schematic representation of regions around the HO cut site on chromosome III. The ChIP probe used in this study is 0.6 kb from the DSB. The *Rsa*I sites used in the qPCR resection assays, 0.15 kb from the DSB, are also indicated. *B*, enrichment of Sae2[HA] at DSB, at 0 and 3 h, in WT (JC-5116), *nej1Δ* (JC-5124), *mre11Δ* (JC-5122), *ku70Δ* (JC-5948), *dnl4Δ* (JC-5946), and a nonepitope-tagged (NT) control (JC-727). The fold enrichment represents normalization over the SMC2 locus. *C*, enrichment of Sae2[HA] at 0.6 kb from DSB, at 0 (no DSB induction), 40, 80, and 150 min after DSB induction in WT (JC-5116) and *nej1Δ* (JC-5124). *D*, enrichment of Nej1[Myc] at DSB, at 0 and 3 h, in WT (JC-1687), *mre11Δ* (JC-3677), *sae2Δ* (JC-5118), and a nonepitope-tagged (NT) control (JC-727). *E*, Y2H analysis of Sae2 fused to HA-AD and Nej1 fused to LexA-DBD in WT cells (JC-1280) and in isogenic cells with *mre11Δ* (JC-6125) using a quantitative β-galactosidase assay. *F*, Y2H analysis of Sae2 fused to HA-AD, and Mre11, Rad50, and Xrs2 fused to LexA-DBD in WT cells (JC-1280) and in isogenic cells with *nej1Δ* (JC-4556) using a quantitative β-galactosidase assay. *G*, 5′ DNA resection 0.15 kb away from the HO-DSB using a qPCR-based approach described in the [Experimental procedures](#) section. Frequency of resection is plotted as % ssDNA at 0, 40, 80, and 150 min post DSB induction in cycling cells in WT (JC-727), *nej1Δ* (JC-1342), *sae2Δ* (JC-5673), and *nej1Δ sae2Δ* (JC-5675). The error bars represent the standard error from experiments performed on biological triplicates. Significance was determined using 1-tailed, unpaired Student's *t* test. All strains marked ($p < 0.05*$; $p < 0.001***$) are compared to WT. ChIP, chromatin immuno-precipitation; DSB, DNA double-strand break; HA, hemagglutinin; Y2H, yeast two-hybrid.

defective in *sgs1Δ exo1Δ* than *sgs1Δ* (Figs. 2*D* and S2*A*), the deletion of *EXO1* did not alter Dna2 recruitment to the DSB (Figs. 2*C* and S2*B*) nor did it reverse the hyper-resection phenotype in *nej1Δ* mutants, even when Mre11 activity was abrogated in *nej1Δ mre11-3* mutants (Fig. S2, *C* and *D*). Furthermore, the recovery of Exo1 did not change in *nej1Δ* like it did when end protection was lost as in *ku70Δ* mutants (Fig. S2*E*). In all, our data suggest that the Sgs1-independent

pathway for Dna2 recruitment, which is also inhibited by Nej1, did not depend on Exo1.

Given the interactions between Nej1 and Sae2, we next measured Sae2 recovery in these various mutants. While Sae2 recruitment was abrogated in *mre11Δ* (Fig. 1*B*), its localization increased in *mre11-3* mutants (Fig. 2*E*), which is consistent with earlier work (28). Conversely, in *sgs1Δ* and *exo1Δ* mutants, Sae2 enrichment remained indistinguishable from
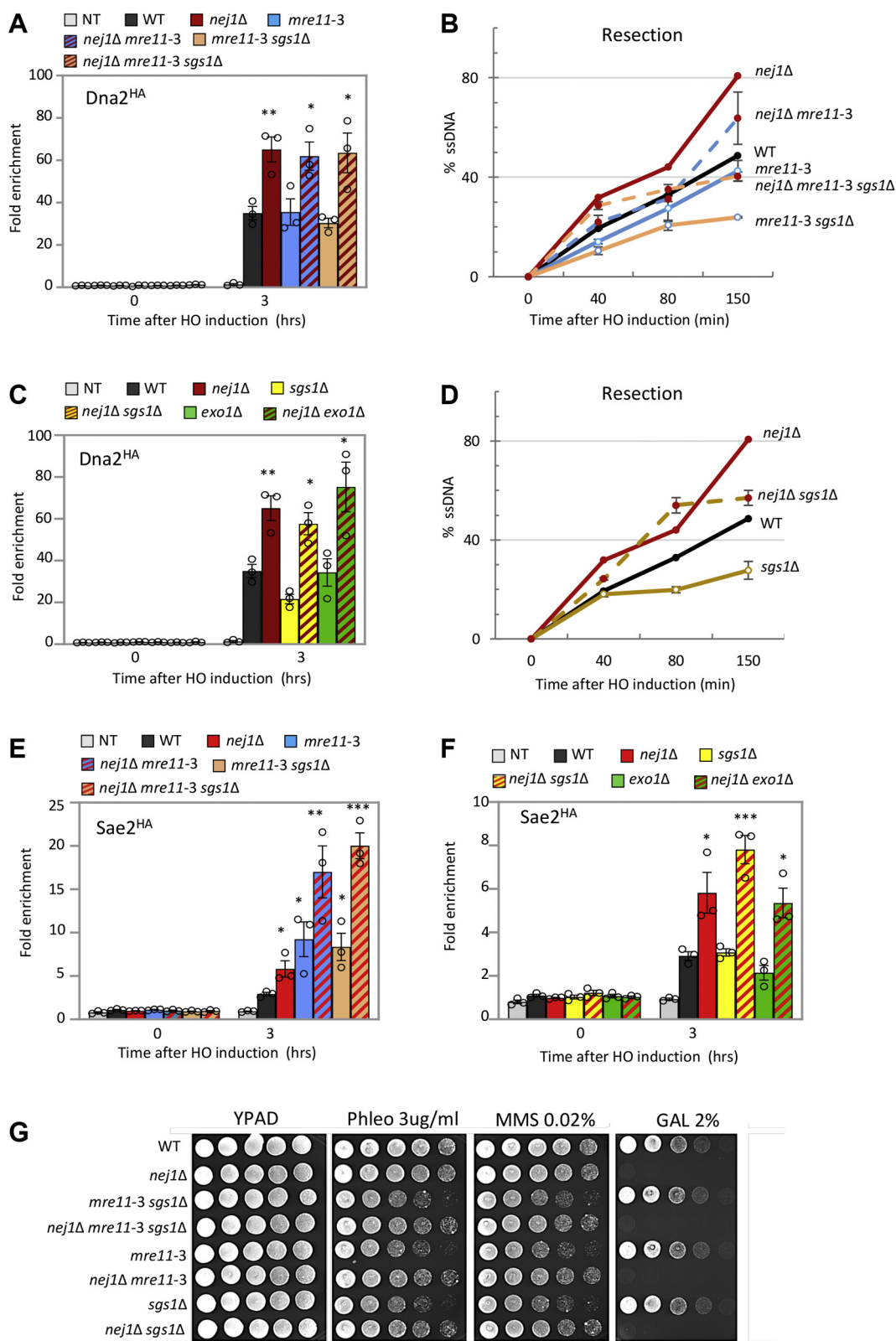
Figure 2. Nej1 regulates resection and HR by inhibiting Dna2 and Sae2. *A* and *C*, enrichment of Dna2[HA] at 0.6 kb from DSB, at 0 and 3 h, after DSB induction in WT (JC-4117), *nej1Δ* (JC-4118), *mre11-3* (JC-5594), *nej1Δ mre11-3* (JC-5596), *mre11-3 sgs1Δ* (JC-5621), *nej1Δ mre11-3 sgs1Δ* (JC-5623), *sgs1Δ* (JC-5624), *nej1Δ sgs1Δ* (JC-5627), *exo1Δ* (JC-5626), *nej1Δ exo1Δ* (JC-5666), and a nonepitope-tagged (NT) control (JC-727) was determined. The fold enrichment is normalized to recovery at the SMC2 locus. *B* and *D*, 5′ DNA resection 0.15 kb away from the HO-DSB using a qPCR-based approach described in the Experimental procedures section. Frequency of resection is plotted as % ssDNA at 0, 40, 80, and 150 min post DSB induction in cycling cells in WT (JC-727), *nej1Δ* (JC-1342), *mre11-3* (JC-5372), *nej1Δ mre11-3* (JC-5369), *mre11-3 sgs1Δ* (JC-5405), *nej1Δ mre11-3 sgs1Δ* (JC-5667), *sgs1Δ* (JC-3757), and *nej1Δ sgs1Δ* (JC-3759). *E* and *F*, enrichment of Sae2[HA] at DSB, at 0 and 3 h, in WT (JC-5116), *nej1Δ* (JC-5124), *mre11-3* (JC-5119), *nej1Δ mre11-3* (JC-5702), *mre11-3 sgs1Δ* (JC-

WT (Fig. 2F). Sae2 recovery in *nej1Δ mre11-3* double mutants was additive, and above levels recovered in either single mutant, and it was also not diminished by the further deletion of *SGS1* (Fig. 2E).

These data suggest that the Sgs1-independent pathway of Dna2 recruitment could involve Sae2 as its association with the DSB was not impacted by *SGS1* deletion (Fig. 2, E and F). Moreover, both Dna2 and Sae2 recovery and 5′ resection were greater in *nej1Δ mre11-3 sgs1Δ* compared to *mre11-3 sgs1Δ* double mutants, highlighting the inhibitor function of Nej1 (Fig. 2, A, B and E). Likewise, cell survival was greater in *nej1Δ mre11-3 sgs1Δ* than *mre11-3 sgs1Δ* mutants plated on phleomycin or methyl methanesulfonate (MMS), two agents that cause DSBs (Fig. 2G). When the HR pathway is the dominant mode of repair, like in these drop assays, increased Dna2 levels and increased resection correlated with increased resistance. By contrast, when one DSB is continuously induced at the HO cut site in cells engineered to preclude HR, survival on GAL serves as a readout of end-joining repair. All mutant combinations with *nej1Δ* showed decreased survival upon continuous DSB induction at the HO recognition site, which underscores the essentiality of Nej1 in end-joining (Fig. 2G).

Nej1 interactions with Sae2 regulate Dna2 recruitment and end-bridging

Resection was lower in *nej1Δ sae2Δ* and *sae2Δ* than *nej1Δ mre11-3* and *mre11-3*, respectively (Figs. 1G and 2B), which is consistent with Sae2 having functions in DSB repair beyond it role of activating Mre11 nuclease (28). Thus, we next determined whether Sae2 was involved in the recruitment of Dna2 to the DSB and whether this was inhibited by Nej1 given the higher levels of both Dna2 and Sae2 recovered in *nej1Δ* and *nej1Δ mre11-3* mutants. Indeed, the increased Dna2 recovery in *nej1Δ mre11-3* double mutants was Sae2 dependent with Dna2 enrichment level in *nej1Δ mre11-3 sae2Δ* being similar to WT (Fig. 3A). Moreover, deletion of *SAE2* also reversed the elevated resection occurring in *nej1Δ mre11-3* mutants (Fig. 3B). The recovery of Dna2 decreased in *sae2Δ* and *mre11-3 sae2Δ* mutant cells even more than it did in *sgs1Δ* and *mre11-3 sgs1Δ* (Fig. 3A). In drop assays, deletion of *NEJ1* in *mre11-3 sae2Δ* mutants showed no greater resistance to phleomycin or MMS than *mre11-3 sae2Δ*, which was in contrast to the increased resistance *nej1Δ* provided in combination with *mre11-3 sgs1Δ* (Fig. 3C). These data suggest there is a correlation between increased Dna2 levels and increased resistance, which occurred in *nej1Δ mre11-3 sgs1Δ* but not in *nej1Δ mre11-3 sae2Δ* mutants (Figs. 2G and 3A).

These data suggest that Sae2 functions with Dna2 to promote resection. Therefore, we determined whether Sae2 and Dna2 physically interacted by Y2H. As previously described,

HA-tagged Sae2 prey was expressed together with LexA-tagged Dna2 baits (Fig. S3A) (4, 41). Sae2 interacted with Dna2^N, which is the N-terminal regulatory region (1–450 aa) and Dna2^{Nuc}, the nuclease domain (451–900 aa; light green bars). Similar to Sae2-MRX, Sae2 interactions with Dna2^N and Dna2^{Nuc} increased in *nej1Δ* mutants (dark green bars; Figs. 3D and S3B). Of note, deletion of *NEJ1* did not increase binding between all proteins combinations expressed from 2-hybrid vectors, as Mre11–Rad50 interactions were unaltered in *nej1Δ* cells and all constructs were similarly expressed in WT and *nej1Δ* backgrounds (Fig. S3, C–E). Taken together with previous work (4), these data suggest that Nej1 functions as a general inhibitor of interactions between nucleases and their binding partners. Nej1 inhibits both Sae2–MRX and Sae2–Dna2 interactions in addition to Dna2–Sgs1 and Dna2–Mre11 interactions (4).

Nej1 is essential for end-joining, therefore in the HO-DSB genetic background, growth on 2% GAL was markedly reduced in all mutant combinations containing *nej1Δ* as seen in drop assays (Figs. 2G and 3C) and by more quantitative cell survival measurements (Table 1). In general, survival on continuous GAL correlated inversely with 5′ DNA resection. The overall survival frequency was very low because only cells that have acquired mutations that prevent recutting can survive (Table 1). However, this assay is useful because determining the mating type of survivors provides insight about DNA processing events that occurred *in vivo* during DSB repair and can reveal information about the types of genomic alterations that develop at the break site. The HO-DSB is located within MATα1 and adjacent to MATα2 (Fig. S4A). Their expression regulates the mating type by activating α-type genes and inhibiting a-type genes. Extensive resection that leads to large deletions (>700 bp) produces 'a-like' survivors because both α1 and α2 are disrupted (9). Consistent with previous reports, large deletions developed in *nej1Δ* (Table 1 and Fig. S4A). The frequency of large genomic deletions that developed in *nej1Δ* survivors was partly reduced by further deleting *SGS1* or *SAE2* (Table 1) and correlated with decreased resection in both double mutants (Figs. 1G and 2D). Large deletions also decreased to a lesser extent in *nej1Δ mre11-3*, but there was no decrease when *EXO1* was deleted in combination with *nej1Δ* (Table 1). Of note, resection remained elevated in *nej1Δ exo1Δ*, similarly to *nej1Δ* mutants (Fig. S2C). Survivors of *nej1Δ mre11-3 sgs1Δ* and *nej1Δ mre11-3 sae2Δ* triples showed a further decrease in the frequency of large deletions compared to *nej1Δ mre11-3* (Table 1 and Fig. S4A). We previously demonstrated that large deletions develop at DSBs when 5′ resection initiates and DNA end-bridging is defective (4). Given Sae2 has a role in end-bridging like MRX and Nej1 (36–38), we wanted to determine how the rate of genomic deletions correlated with 5′ resection and end-bridging defects in the various mutant combinations.

🔷 ASBMB

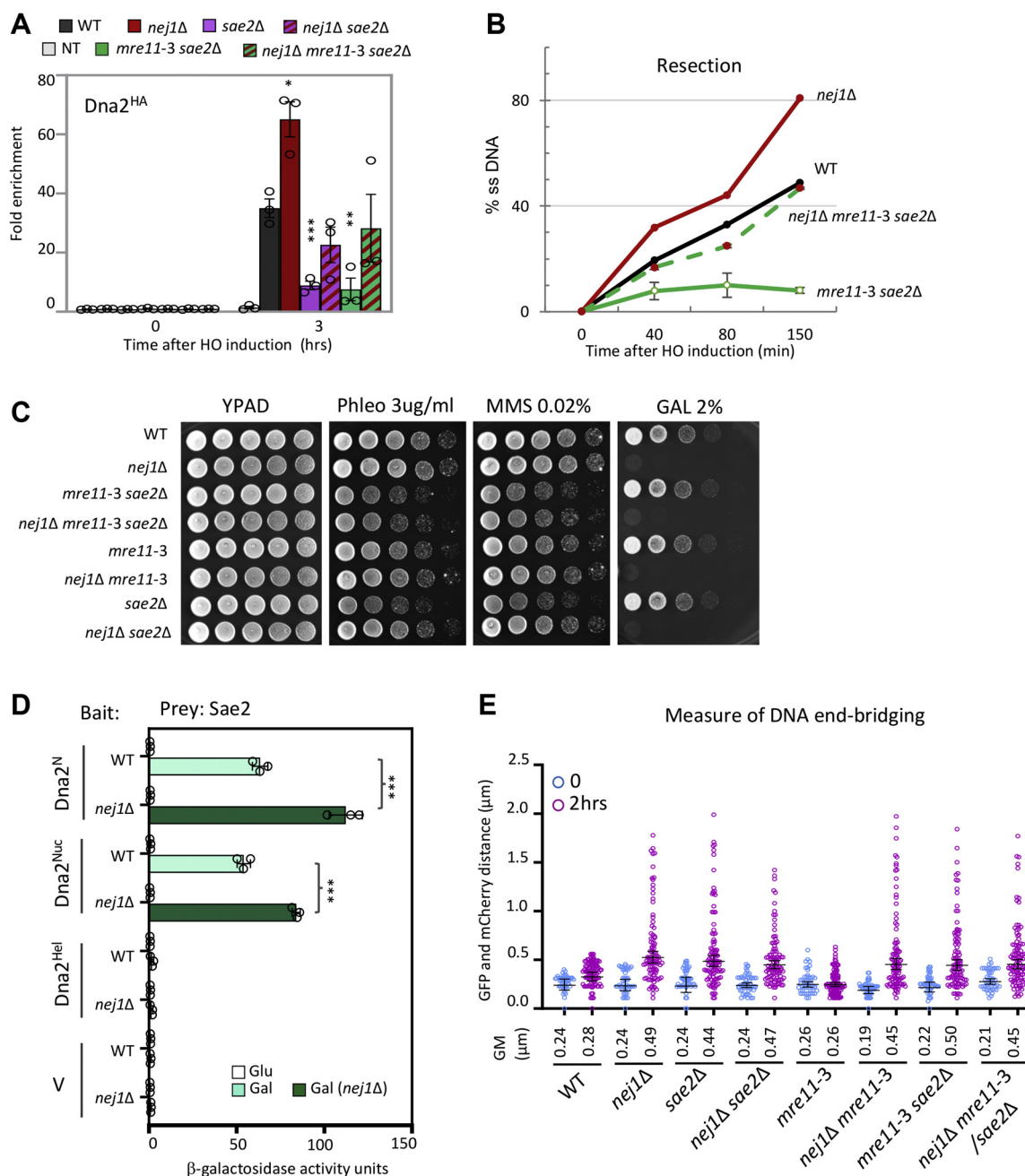*J. Biol. Chem.* (2022) 298(6) 101937 **5**

Figure 3. Sae2-dependent recruitment of Dna2 is inhibited by Nej1. *A,* enrichment of Dna2^{HA} at 0.6 kb from DSB 0 h (no DSB induction) and 3 h after DSB induction in WT (JC-4117), *nej1Δ* (JC-4118), *sae2Δ* (JC-5562), *nej1Δ sae2Δ* (JC-5597), *mre11-3 sae2Δ* (JC-5598), *nej1Δ mre11-3 sae2Δ* (JC-5593), and a nonepitope-tagged (NT) control (JC-727) was determined. The fold enrichment is normalized to recovery at the SMC2 locus. *B,* 5′ DNA resection 0.15 kb away from the HO-DSB using a qPCR-based approach described in the [Experimental procedures](#) section. Frequency of resection is plotted as % ssDNA at 0, 40, 80, and 150 min post DSB induction in cycling cells in WT (JC-727), *nej1Δ* (JC-1342), *mre11-3 sae2Δ* (JC-5501), and *nej1Δ mre11-3 sae2Δ* (JC-5500). *C,* five-fold serial dilutions of the cells in WT (JC-727), *nej1Δ* (JC-1342), *mre11-3 sae2Δ* (JC-5501) and *nej1Δ mre11-3 sae2Δ* (JC-5500), *mre11-3* (JC-5372), *nej1Δ mre11-3* (JC-5369), *sae2Δ* (JC-5673), and *nej1Δ sae2Δ* (JC-5675) were spotted on YPAD, 3.0 μg/ml phleomycin, 0.02% MMS, and 2% GAL. *D,* Y2H analysis of Sae2 fused to HA-AD and domains of Dna2, (Dna2-N terminal, Dna2-Nuclease, and Dna2-Helicase domains) fused to LexA-DBD was performed in WT cells (JC-1280) and in isogenic cells with *nej1Δ* (JC-4556) using a quantitative β-galactosidase assay. *E,* scatter plot showing the tethering of DSB ends, at 0 and 2 h, as measured by the distance between the GFP and mCherry foci in WT (JC-4066), *nej1Δ* (JC-4364), *sae2Δ* (JC-5524), *nej1Δ sae2Δ* (JC-5525), *mre11-3* (JC-5529), *nej1Δ mre11-3* (JC-5526), *mre11-3 sae2Δ* (JC-5530), and *nej1Δ mre11-3 sae2Δ* (JC-5531). The Geometric mean (GM) distance for each sample is specified under the respective sample data plot. Significance was determined using Kruskal-Wallis and Dunn's multiple comparison test. DSB, DNA double-strand break; HA, hemagglutinin. The error bars represent the standard error from experiments performed on biological triplicates. All strains marked ($p < 0.05*$; $p < 0.01**$; $p < 0.001***$) are compared to WT.

End-bridging was measured in cells where both sides of the DSB were tagged with fluorescent markers. The TetO array and the LacO array were integrated 3.2 kb and 5.2 kb, respectively, from the DSB in cells expressing TetR^{GFP} and LacO^{mCherry} fusions, enabling us to visualize both sides by fluorescence microscopy ([Fig. S4*B*](#)). In asynchronous cells, the distance between the GFP and mCherry foci was measured 2 h after DSB induction. In WT cells, the mean distance between

Table 1
Survival and percentage of large deletions during continuous HO-induction

Genotype	Survival	SD (+/−)	Survival relative to WT (%)	Large deletions (%)
WT	2.9×10^{-3}	5.5×10^{-4}	100%	1
$nej1\Delta$	2.0×10^{-5}	1.0×10^{-5}	0.68%	13
$sae2\Delta$	8.2×10^{-3}	6.5×10^{-4}	278%	0
$nej1\Delta\ sae2\Delta$	5.4×10^{-5}	4.4×10^{-5}	1.84%	5
$exo1\Delta$	4.1×10^{-3}	4.1×10^{-4}	141%	0
$nej1\Delta\ exo1\Delta$	1.6×10^{-5}	5.5×10^{-6}	0.53%	12
$mre11$-3	4.5×10^{-3}	5.0×10^{-4}	154%	0
$nej1\Delta\ mre11$-3	3.5×10^{-5}	3.0×10^{-5}	1.21%	8
$sgs1\Delta$	4.1×10^{-3}	1.3×10^{-3}	139%	0
$nej1\Delta\ sgs1\Delta$	1.6×10^{-5}	5.5×10^{-6}	0.56%	6
$mre11$-3 $sgs1\Delta$	4.1×10^{-3}	1.5×10^{-3}	140%	0
$nej1\Delta\ mre11$-3 $sgs1\Delta$	2.6×10^{-5}	5.3×10^{-6}	0.89%	3
$mre11$-3 $sae2\Delta$	8.3×10^{-3}	2.2×10^{-4}	282%	0
$nej1\Delta\ mre11$-3 $sae2\Delta$	6.7×10^{-5}	2.9×10^{-5}	2.28%	7
$nej1\Delta\ sae2\Delta\ sgs1\Delta$	1.3×10^{-5}	2.1×10^{-6}	0.46%	10

the fluorescent markers was not significantly different after HO cutting (0.28 μm) compared to before GAL induction (0.24 μm; Fig. 3E). By contrast, after DSB induction, the distance between markers increased in $sae2\Delta$ mutant cells (0.44 μm), indicating a defect in end-bridging (Fig. 3E). The disruption of end-bridging was not connected to the loss of Mre11 activation accompanying $sae2\Delta$ mutants, as end-bridging in $mre11$-3 (0.26 μm) was similar to WT after inducing a DSB. Furthermore, there was no significant increase in the distance between markers after DSB induction in $sgs1\Delta$ or $exo1\Delta$ mutants (Fig. S4B). Interestingly, deletion of *SAE2* and *NEJ1* showed an epistatic relationship, as the end-bridging defect in the double mutant cells was similar to the defect in each single mutant (Fig. 3E). In all, the defect in end-bridging together with increased 5′ resection in $nej1\Delta\ sae2\Delta$ supports our model that both events correlate with and contribute to the formation of large deletions (Table 1 and Fig. 1G).

NEJ1 *alleviates the SL of* sae2Δ sgs1Δ

We observed that recruitment of Dna2 to DSBs was partially dependent on Sae2 and Sgs1 and that both pathways were inhibited by Nej1. This prompted us to determine whether deletion of *NEJ1* would alleviate the SL of $sae2\Delta\ sgs1\Delta$ (28). We crossed $nej1\Delta\ sae2\Delta$ with $nej1\Delta\ sgs1\Delta$ and spores with the triple mutant combination grew remarkably well (Fig. 4A). The triple mutants showed reduced survival under conditions of continuous HO-DSB induction, similarly to all other mutant combination containing $nej1\Delta$ (Table 1). The frequency of large deletions in $nej1\Delta\ sae2\Delta\ sgs1\Delta$ survivors was slightly higher than in double mutant combinations (Table 1 and Fig. S4A). However, the sensitivity of triple mutants to phleomycin and MMS was similar to that of $nej1\Delta\ sae2\Delta$ and $nej1\Delta\ sgs1\Delta$ double mutants (Fig. 4B). Strikingly, resection in the triple mutants was similar to WT and significantly higher than in $sae2\Delta$ and $sgs1\Delta$ single mutants (Figs. 1G, 2D and 4C). Moreover, Dna2 recovery at the DSB in $nej1\Delta\ sae2\Delta\ sgs1\Delta$ mutants was similar to $nej1\Delta\ sgs1\Delta$ and was higher than recovery in $sae2\Delta \pm NEJ1$ or in $sgs1\Delta$ single mutants (Figs. 2C, 3A and 4D).

To determine whether suppression of $sae2\Delta\ sgs1\Delta$ lethality by *NEJ1* deletion required Dna2 nuclease activity, we generated heterozygous diploids for *SAE2+/sae2Δ*, *SGS1+/sgs1Δ*, *NEJ1+/nej1Δ*, and nuclease-deficient *DNA2+/dna2*-1 (P504→S) and upon tetrad dissection, recovered no viable spores with quadruple mutant combination (Fig. 4E). By contrast, $nej1\Delta\ sae2\Delta\ sgs1\Delta\ exo1\Delta$ spores were viable, thus suppression of $sae2\Delta\ sgs1\Delta$ SL by $nej1\Delta$ depends on the nuclease activity of Dna2, not Exo1 (Fig. S5A). Resection in $dna2$-1 and $dna2\Delta\ pif1$-m2 was similar to each other and more defective than resection in $sgs1\Delta$ mutants (Figs. 4F and S5B). Taken together, these data demonstrate interactions between Dna2 and Sae2 at DSBs were important for 5′ DNA resection independently of Sgs1 and were inhibited by Nej1.

Discussion

Our work strongly suggests that Nej1 operates as a general inhibitor of 5′ resection at DSBs. Not only does Nej1 inhibit Dna2 interactions with Sgs1 and MRX (4), but it physically interacts with Sae2, inhibiting both MRX-dependent recruitment of Sae2 and Sae2-dependent recruitment of Dna2 to the DSB. Our data support a model whereby Dna2 is recruited to a DSB through three pathways, all of which are inhibited by Nej1 (Fig. 5; panel A). Dna2 localizes primarily through binding with Sgs1 or Sae2, thus deleting both results in lethality as Nej1 is present to block Dna2–Mre11 interactions (Fig. 5; panel B). Removal of Nej1 allows Dna2 recruitment through Mre11-Dna2, which suppresses $sae2\Delta\ sgs1\Delta$ SL (4, 28). Sae2 can initiate resection through Mre11 activation, but in the absence of Mre11 nuclease activity and Sgs1 helicase, it can initiate resection through interactions with Dna2. Our data show that Sae2 can compensate for $sgs1\Delta$ to localize Dna2 to DSBs. However, if both *SAE2* and *SGS1* are deleted, Mre11 is critical for Dna2 recovery but it remains blocked by Nej1, therefore Dna2 recruitment occurs when *NEJ1* is also deleted (4). Consistent with this model, the viability of $nej1\Delta\ sae2\Delta\ sgs1\Delta$ triple mutant depends on the nuclease activity of Dna2. After resection initiates, Ku dissociates and Exo1 is present to serve as the nuclease in long-range resection (Fig. 5; panel C).

Sae2-dependent recruitment of Dna2 is inhibited by Nej1

Dna2 localization to DSBs is partly, but not entirely, dependent on Sgs1 helicase (Fig. 2, A and C). An alternative mode of Dna2 recruitment involves Sae2 (Fig. 3A, (19)). Our
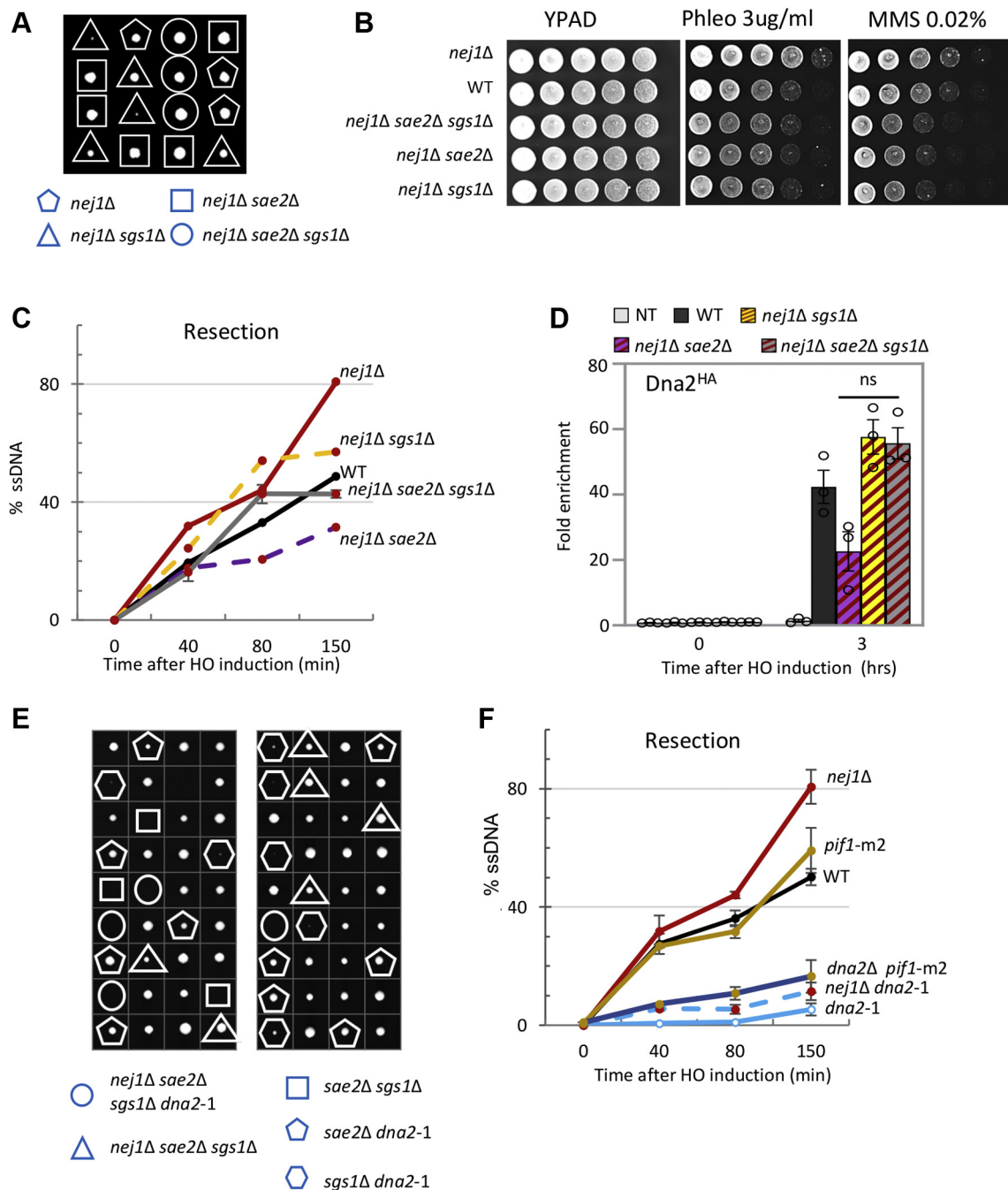
Figure 4. *NEJ1* alleviates the synthetic lethality of *sae2Δ sgs1Δ*. *A*, viability and genotypes of spores derived from diploids of *nej1Δ sae2Δ* (JC-5675) and *nej1Δ sgs1Δ* (JC-3885). *B*, five-fold serial dilutions of *nej1Δ* (JC-1342), WT (JC-727), *nej1Δ sae2Δ sgs1Δ* (JC-5750), *nej1Δ sae2Δ* (JC-5675), and *nej1Δ sgs1Δ* (JC-3759) cells were spotted on YPAD, phleomycin 3.0 μg/ml, and MMS 0.02%. *C*, 5′ DNA resection 0.15 kb away from the HO-DSB using a qPCR-based approach described in the Experimental procedures section. Frequency of resection is plotted as % ssDNA at 0, 40, 80, and 150 min post DSB induction in cycling cells in WT (JC-727), *nej1Δ* (JC-1342), *nej1Δ sae2Δ* (JC-5675), *nej1Δ sgs1Δ* (JC-3759), and *nej1Δ sae2Δ sgs1Δ* (JC-5750). *D*, enrichment of Dna2^HA at 0.6 kb from DSB 0 and 3 h after DSB induction in WT (JC-4117), *nej1Δ sae2Δ* (JC-5597), *nej1Δ sgs1Δ* (JC-5627), *nej1Δ sae2Δ sgs1Δ* (JC-5480), and a nonepitope-tagged (NT) control (JC-727) was determined. The fold enrichment is normalized to recovery at the SMC2 locus. *E*, viability and genotypes of spores derived from heterozygous diploids of *SAE2*+/*sae2Δ*, *SGS1*+/*sgs1Δ*, *NEJ1*+/*nej1Δ*, and *DNA2*+/*dna2*-1 generated from a cross between JC-5749 and JC-5655. *F*, 5′ DNA resection 0.15 kb away from the HO-DSB using a qPCR-based approach described in the Experimental procedures section. Frequency of resection is plotted as % ssDNA at 0, 40, 80, and 150 min post DSB induction in cycling cells in WT (JC-727), *nej1Δ* (JC-1342), *dna2*-1 (JC-5655), *nej1Δ dna2*-1 (JC-5670), *pif1*-m2 (yWH0056), and *dna2Δ pif1*-m2 (yWH0055). The *pif1*-m2 and *dna2Δ pif1*-m2 strains in the same background were a kind gift from Greg Ira's laboratory, Baylor College of Medicine. DSB, DNA double-strand break; HA, hemagglutinin. Experiments were performed on biological triplicates.

results provide mechanistic insight for *in vitro* studies where CtIP stimulates Dna2 nuclease and support previous work showing a role for human CtIP in Dna2 recruitment to DSBs (33–35). Although our findings differ slightly from previous work, which showed little decrease in Dna2 recovery 3 h after DSB induction, the discrepancy could stem from slight variations in experimental design because in the same study, Dna2 was reduced 2 h after DSB induction in *sae2Δ* mutants (19).
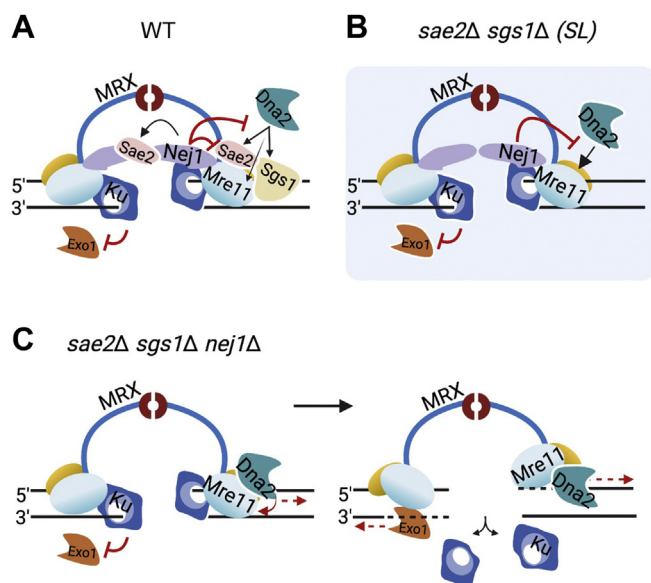
Figure 5. Interplay of Nej1, Sae2 and Sgs1 at DSB. Model of DSB where Nej1 prevents Mre11-dependent Dna2 recruitment to DSB. *A*, in WT cells, Nej1 inhibits Dna2 recruitment *via* Mre11, Sae2, and Sgs1. *B*, in *sae2Δ sgs1Δ* mutant cells, Nej1 inhibits Dna2–Mre11 interaction and therefore prevents the residual Dna2 recruitment and resection, resulting into the synthetic lethality. *C*, upon *NEJ1* deletion, Dna2 can get recruited through Mre11 leading to resection and repair, resulting into alleviation of the synthetic lethality and growth of *nej1Δ sae2Δ sgs1Δ* cells. Created with BioRender. com. DSB, DNA double-strand break.

By ChIP, the Sgs1-independent pathways of Dna2 localization, involving Sae2 and Mre11 were robustly inhibited by Nej1 (Figs. 2C and 3A; (4)). Our Y2H data support this, as physical interactions between Dna2 and Sae2, and Dna2 and Mre11 increased in *nej1Δ* mutant cells (Fig. 3C). The localization of MRX to DSBs was not disrupted in nuclease-deficient *mre11*-3 mutants (12, 13), which was important as the MRX complex was needed for the recruitment of all the processing factors we investigated here. Using the *mre11*-3 allele, we could also see that Dna2 recovery and resection trends were not significantly affected by the disruption of Mre11 nuclease activity.

Highlighting previous work proposing Sae2 has a role at DSBs in addition to Mre11 activation, we saw a marked decrease in resection in *sae2Δ* compared to *mre11*-3 mutants, which can be attributed to the decreased recovery of Dna2 in *sae2Δ* compared to *mre11*-3 mutants. Given the importance of Sae2 in Dna2 localization (Fig. 3A), resection could even be supported by increased Sae2 levels in *mre11*-3 mutants ± *SGS1* (Fig. 2, *B* and *E* and (28)). Furthermore, our data also complemented earlier work that showed decreased resection in *sae2Δ* mutants resulted from increased end-protection by Ku (19). Ku is important for Nej1 recruitment, therefore, it is noteworthy that increased Ku did not result in increased Nej1 recovery in *sae2Δ* (Figs. 1D and S1A). Lastly, resection differences observed when comparing *sae2Δ* and *mre11*-3 mutants might also be related to checkpoint signaling defects in *sae2Δ* mutants, defects that are independent of Mre11 nuclease activity (28). Our data do not address whether Nej1 inhibits Sae2 nuclease functions (29), and further studies

involving Nej1 and Dna2 with Sae2-mutants (D285P/K288P and E161P/K163P) will be needed to investigate this directly.

Nej1 and Sae2 in DNA end-bridging

Deletion of *NEJ1* and *SAE2* show epistatic end-bridging defects raising the possibility that Nej1 and Sae2 collaborate to restrain movement of the broken DNA ends at DSBs in contrast to their antagonistic roles in resection. Given the physical interaction between Nej1 and Sae2, which existed independently of Mre11, the two factors could potentially function together in end-bridging (Figs. 1E and 3E). Additional work will be required to determine whether there is a sub-population of Sae2 involved in DNA end-bridging apart from Sae2 homo-oligomers involved in Mre11 activation and checkpoint signaling (46, 47). DNA end-bridging was maintained in *mre11*-3 mutants, which is in line with previous work showing that the structural integrity of the MRX complex, but not its nuclease activity, is important for bridging (4, 12, 13, 48). Comparing end-bridging defects in *mre11*-3 and *sae2Δ* mutants ± *NEJ1* supports the model that large deletions develop when 5′ resection proceeds and end-bridging is disrupted. In *mre11*-3 mutants, 5′ resection proceeds but end-bridging was not disrupted, whereas in *sae2Δ* mutants, bridging was disrupted but 5′ resection was very low and neither single mutant showed large deletions (Table 1 and (12, 13, 36–38)). By contrast, large deletions formed when either mutant was combined with *nej1Δ*, although the frequency was lower than *nej1Δ* single mutants (Table 1).

SL of *sae2Δ sgs1Δ* is supressed by *NEJ1* deletion

Suppression of *sae2Δ sgs1Δ* SL by *nej1Δ* was dependent on Dna2, but not Exo1 nuclease activity (Figs. 4F and S4) (28). Moreover, the higher rate of resection in *sgs1Δ* mutants than *dna2Δ pif1*-m2 and *dna2*-1 mutants also demonstrates the importance of Dna2 in DSB repair, independently of Sgs1. While both Dna2 and Sgs1 have important links to the DNA damage checkpoint (49), the greater resection defect in *dna2*-1 is likely not attributed to its checkpoint functions as mutations in Dna2 that disrupt signaling map to its N-terminal region, distinct of its nuclease and helicase activities (50). In addition, 5′ resection was similarly reduced in *dna2*-1 and *dna2Δ pif1*-m2 mutants (Fig. 4D), excluding a potential dominant-negative effect for *dna2*-1 in tetrad analysis.

Surprisingly, the frequency of 5′ resection and the recovery level of Dna2 in *nej1Δ sae2Δ sgs1Δ* triple mutants was similar to WT and above *nej1Δ sae2Δ* (Fig. 4, C and D), suggesting that Sgs1 could even be inhibitory to Dna2 recruitment in *nej1Δ sae2Δ* double mutant cells. We previously showed that both Sgs1 and Dna2 interact directly with Mre11 (4), thus in *nej1Δ sae2Δ* mutants, the presence of Sgs1 could inhibit the initiation of resection occurring from Dna2–Mre11 interactions. The presence of Sgs1, and therefore Dna2–Sgs1 complex formation, might be less efficient at initiating resection than its abilities in long-range resection. Like with *nej1Δ*, previous work showed that *ku70Δ* and *rad9Δ* also suppressed *sae2Δ sgs1Δ* lethality (20, 28). This raises the possibility that

suppression of *sae2Δ sgs1Δ* lethality might result from a decrease in overall NHEJ when *NEJ1* was also deleted. However, two results argue that intrinsic loss of NHEJ itself does not suppress this lethality. First, deletion of *DNL4* ligase does not rescue *sae2Δ sgs1Δ* and second, NHEJ occurs in *rad9Δ sae2Δ sgs1Δ* triple mutants (20, 28). Taken together, our work provides new information on how Nej1 inhibits nuclease recruitment and 5′ resection at DSBs. These functions help preserves genome integrity during repair pathway choice and ascribe a wider range of responsibilities to Nej1 that are distinct of its roles in canonical NHEJ.

Experimental procedures

All the yeast strains used in this study are listed in Table S3 and were obtained by crosses. The strains were grown on various media in experiments described below. For HO induction of a DSB, YPLG media is used (1% yeast extract, 2% bacto peptone, 2% lactic acid, 3% glycerol, and 0.05% glucose). For the continuous DSB assay, YPA plates are used (1% yeast extract, 2% bacto peptone, 0.0025% adenine) supplemented with either 2% glucose (GLU) or 2% GAL. For the mating type assays, YPAD plates are used (1% yeast extract, 2% bacto peptone, 0.0025% adenine, 2% dextrose). For Y2H assays, standard amino acid drop-out media lacking histidine, tryptophan, and uracil is used and 2% raffinose is added as the carbon source for the cells.

Chromatin immunoprecipitation

ChIP was performed as described previously (4). Cells were cultured overnight in YPLG at 25 °C. Cells were then diluted to 5×10^6 cells/ml and cultured to one doubling (3–4 h) at 30 °C. Two percent GAL was added to the YPLG media and cells were harvested and crosslinked at various time points using 3.7% formaldehyde solution. Following crosslinking, the cells were washed with ice cold PBS and the pellet stored at −80 °C. The pellet was resuspended in lysis buffer (50 mM Hepes pH 7.5, 1 mM EDTA, 80 mM NaCl, 1% Triton, 1 mM PMSF, and protease inhibitor cocktail) and cells were lysed using Zirconia beads and a bead beater. Chromatin fractionation was performed to enhance the chromatin bound nuclear fraction by spinning the cell lysate at 13,200 rpm for 15 min. The pellet was resuspended in lysis buffer and sonicated to yield DNA fragments (∼500 bps in length). The sonicated lysate was then incubated with αHA- or αMyc- antibody conjugated beads or unconjugated beads (control) for 2 h at 4 °C. The beads were washed using wash buffer (100 mM Tris, pH 8, 250 mM LiCl, 150 mM (αHA) or 500 mM (αMyc) NaCl, 0.5% NP-40, 1 mM EDTA, 1 mM PMSF, and protease inhibitor cocktail), and protein–DNA complexes were released by reverse crosslinking using 1% SDS in TE buffer, followed by proteinase K treatment and DNA isolation *via* phenol-chloroform-isoamyl alcohol extraction. Quantitative PCR was performed using the Applied Biosystem QuantStudio 6 Flex machine. PerfeCTa qPCR SuperMix, ROX was used to visualize enrichment at HO2 (0.5 kb from DSB) and HO1 (1.6 kb from DSB), and SMC2 was used as an internal control. HO cutting was measured in strains used to perform ChIP in Table S2.

Microscopy to determine DNA end-bridging

Cells derived from the parent strain JC-4066 were diluted and grown overnight in YPLG at 25 °C to reach a concentration of 1×10^7 cells/ml. Cells were treated with 2% GAL for 2 h and cell pellets were collected and washed two times with PBS. After the final wash, cells were placed on cover slips and imaged using a fully motorized Nikon Ti Eclipse inverted epifluorescence microscope. Z-stack images were acquired with 200 nm increments along the z plane, using a 60× oil immersion 1.4 N.A. objective. Images were captured with a Hamamatsu Orca flash 4.0 v2 sCMOS 16 bit camera, and the system was controlled by Nikon NIS-Element Imaging Software (Version 5.00). All images were deconvolved with Huygens Essential version 18.10 (Scientific Volume Imaging, http://svi.nl), using the Classic Maximum Likelihood Estimation algorithm, with SNR:40 and 50 iterations. To measure the distance between the GFP and mCherry foci, the ImageJ plugin Distance Analysis was used (51). Distance measurements represent the shortest distance between the brightest pixel in the mCherry channel and the GFP channel. Each cell was measured individually and >50 cells were analyzed per condition per biological replicate.

qPCR-based resection assay

Cells from each strain were grown overnight in 15 ml YPLG to reach an exponentially growing culture of 1×10^7 cells/ml. Next, 2.5 ml of the cells were pelleted as timepoint 0 sample, and 2% GAL was added to the remaining cells to induce a DSB. Following that, respective timepoint samples were collected. Genomic DNA was purified using standard genomic preparation method by isopropanol precipitation and ethanol washing, and DNA was resuspended in 100 ml ddH$_2$O. Genomic DNA was treated with 0.005 μg/μl RNase A for 45 min at 37 °C. Two microliters of DNA was added to tubes containing CutSmart buffer with or without *Rsa*I restriction enzyme and incubated at 37 °C for 2 h. Quantitative PCR was performed using the Applied Biosystem QuantStudio 6 Flex machine. PowerUp SYBR Green Master Mix was used to quantify resection at MAT1 (0.15 kb from DSB) locus. Pre1 was used as a negative control and the % resected/cut HO loci is reported from the amount of *Rsa*I cut DNA normalized to the level of HO cutting at each timepoint (Table S1) (36).

Continuous DSB assay and identification of mutations in survivors

Cells were grown overnight in YPLG media at 25 °C to saturation. Cells were collected by centrifugation at 2500 rpm for 3 min, and pellets were washed 1× in ddH$_2$O and resuspended in ddH$_2$O. Cells were counted and spread on YPA (1% yeast extract, 2% bacto peptone, 0.0025% adenine) plates supplemented with either 2% GLU or 2% GAL. On the GLU plates, 1×10^3 total cells were added and on the GAL plates,

1×10^5 total cells were added. The cells were incubated for 3 to 4 days at room temperature and colonies counted on each plate. Survival was determined by normalizing the number of surviving colonies on the GAL plates to number of colonies on the GLU plates. One hundred survivors from each strain were scored in the mating type assay as previously described (9).

Yeast 2-hybrid

Various plasmids (Table S4) were constructed containing the gene encoding the region of the proteins—Sae2, Dna2, Mre11, Nej1, Rad50 and Xrs2—using the primers listed in Table S5. The plasmids J-965 and J-1493 and the inserts were treated with *BamH*I and *EcoR*I and ligated using T4 DNA ligase. The plasmids were sequence verified. Reporter (J-359), bait (J-965), and prey (J-1493) plasmids, containing the gene encoding the desired protein under a GAL inducible promoter, were transformed into JC-1280. Cells were grown overnight in −URA −HIS −TRP media with 2% raffinose and the next day were transferred into −URA −HIS −TRP media with either 2% GLU or 2% GAL and grown for 6 h at 30 °C. Cell pellets were resuspended and then permeabilized using 0.1% SDS followed by ONPG addition. β-galactosidase activity was estimated by measuring the absorbance at 420 nm, and relative β-galacto-sidase units were determined by normalizing to total cell density A600. For drop assay, cells were grown and spotted in five-fold serial dilutions on plates containing 2% GAL lacking histidine and tryptophan (for plasmid selection) and leucine (for measuring expression from *lexAop6-LEU2*). Plates were photographed after 3 to 4 days of incubation at 30 °C.

Western blots

Cells were lysed by resuspending them in lysis buffer (with PMSF and protease inhibitor cocktail tablets) followed by bead beating. The protein concentration of the whole cell extract was determined using the NanoDrop. Equal amounts of whole cell extract were added to wells of 10% polyacrylamide SDS gel. After the run, proteins were transferred to Nitrocellulose membrane at 100 V for 80 min. The membrane was Ponceau stained (which served as a loading control), followed by blocking in 10% milk-PBST for 1 h at room temperature. The respective primary antibody solution (1:1000 dilution) was then added and incubated overnight at 4 °C, followed by washing with PBST. The secondary antibody was left for 1 h. The membranes were then washed with PBST and left for 1 h with secondary antibody, followed by washing and performing ECL detection and followed by washing the membranes, adding the ECL substrates, and imaging them.

Tetrad analysis

Diploids of *nej1Δ sae2Δ* (JC-5675) X *nej1Δ sgs1Δ* (JC-3885) (Fig. 4A) and *nej1Δ sae2Δ sgs1Δ* (JC-5749) X *dna2*-1 (JC-5655) (Fig. 4E) were sporulated. The spores were checked by replica-plating on the marker plates (*-HIS*, +NAT, +KAN, and 37 °C). (*sae2Δ::HIS3*, *sgs1Δ::NatRMX4 nej1Δ::KanMX6*, *dna2*-1, which is temperature sensitive). For analysis, two-two gene

segregation was observed among the tetrads. The tetrad scoring data is available with the article.

DSB efficiency

The efficiency of HO cutting was measured as previously described at all timepoints in the 5′ resection experiments (9). Cells were grown in YPLG before the addition of GAL to induce expression of the HO endonuclease, leading to DSB formation. The cells were pelleted and gDNA was prepared followed by qPCR with a primer set flanking the DSB (HO6 primers, Table S5).

Data availability

All data are contained within the article and all reagents are available upon request.

References

1. Wu, D., Topper, L. M., and Wilson, T. E. (2008) Recruitment and dissociation of nonhomologous end joining proteins at a DNA double-strand break in *Saccharomyces cerevisiae*. *Genetics* **178**, 1237–1249
2. Palmbos, P. L., Wu, D., Daley, J. M., and Wilson, T. E. (2008) Recruitment of *Saccharomyces cerevisiae* Dnl4-Lif1 complex to a double-strand break requires interactions with Yku80 and the Xrs2 FHA domain. *Genetics* **180**, 1809–1819

3. Chen, X., and Tomkinson, A. E. (2011) Yeast Nej1 is a key participant in the initial end binding and final ligation steps of nonhomologous end joining. *J. Biol. Chem.* **286**, 4931–4940

4. Mojumdar, A., Sorenson, K., Hohl, M., Toulouze, M., Lees-Miller, S. P., Dubrana, K., and Cobb, J. A. (2019) Nej1 interacts with Mre11 to regulate tethering and Dna2 binding at DNA double-strand breaks. *Cell Rep.* **28**, 1564–1573.e3

5. Frank-Vaillant, M., and Marcand, S. (2001) NHEJ regulation by mating type is exercised through a novel protein, Lif2p, essential to the ligase IV pathway. *Genes Dev.* **15**, 3005–3012

6. Valencia, M., Bentele, M., Vaze, M. B., Herrmann, G., Kraus, E., Lee, S. E., Schär, P., and Haber, J. E. (2001) NEJ1 controls non-homologous end joining in *Saccharomyces cerevisiae*. *Nature* **414**, 666–669

7. Zhang, Y., Hefferin, M. L., Chen, L., Shim, E. Y., Tseng, H. M., Kwon, Y., Sung, P., Lee, S. E., and Tomkinson, A. E. (2007) Role of Dnl4-Lif1 in nonhomologous end-joining repair complex assembly and suppression of homologous recombination. *Nat. Struct. Mol. Biol.* **14**, 639–646

8. Mahaney, B. L., Lees-Miller, S. P., and Cobb, J. A. (2014) The C-terminus of Nej1 is critical for nuclear localization and non-homologous end-joining. *DNA Repair (Amst.)* **14**, 9–16

9. Sorenson, K. S., Mahaney, B. L., Lees-Miller, S. P., and Cobb, J. A. (2017) The non-homologous end-joining factor Nej1 inhibits resection mediated by Dna2-Sgs1 nuclease-helicase at DNA double strand breaks. *J. Biol. Chem.* **292**, 14576–14586

10. Hopfner, K. P., Karcher, A., Craig, L., Woo, T. T., Carney, J. P., and Tainer, J. A. (2001) Structural biochemistry and interaction architecture of the DNA double-strand break repair Mre11 nuclease and Rad50-ATPase. *Cell* **105**, 473–485

11. Wiltzius, J. J., Hohl, M., Fleming, J. C., and Petrini, J. H. (2005) The Rad50 hook domain is a critical determinant of Mre11 complex functions. *Nat. Struct. Mol. Biol.* **12**, 403–407

12. Hohl, M., Kwon, Y., Galván, S. M., Xue, X., Tous, C., Aguilera, A., Sung, P., and Petrini, J. H. (2011) The Rad50 coiled-coil domain is indispensable for Mre11 complex functions. *Nat. Struct. Mol. Biol.* **18**, 1124–1131

13. Hohl, M., Kochańczyk, T., Tous, C., Aguilera, A., Krężel, A., and Petrini, J. H. (2015) Interdependence of the rad50 hook and globular domain functions. *Mol. Cell* **57**, 479–491

14. Symington, L. S. (2016) Mechanism and regulation of DNA end resection in eukaryotes. *Crit. Rev. Biochem. Mol. Biol.* **51**, 195–212

15. Cannavo, E., and Cejka, P. (2014) Sae2 promotes dsDNA endonuclease activity within Mre11-Rad50-Xrs2 to resect DNA breaks. *Nature* **514**, 122–125

16. Cejka, P. (2015) DNA end resection: Nucleases team up with the right partners to initiate homologous recombination. *J. Biol. Chem.* **290**, 22931–22938

17. Zhu, Z., Chung, W. H., Shim, E. Y., Lee, S. E., and Ira, G. (2008) Sgs1 helicase and two nucleases Dna2 and Exo1 resect DNA double-strand break ends. *Cell* **134**, 981–994

18. Mimitou, E. P., and Symington, L. S. (2008) Sae2, Exo1 and Sgs1 collaborate in DNA double-strand break processing. *Nature* **455**, 770–774

19. Shim, E. Y., Chung, W. H., Nicolette, M. L., Zhang, Y., Davis, M., Zhu, Z., Paull, T. T., Ira, G., and Lee, S. E. (2010) *Saccharomyces cerevisiae* Mre11/Rad50/Xrs2 and Ku proteins regulate association of Exo1 and Dna2 with DNA breaks. *EMBO J.* **29**, 3370–3380

20. Mimitou, E. P., and Symington, L. S. (2010) Ku prevents Exo1 and Sgs1-dependent resection of DNA ends in the absence of a functional MRX complex or Sae2. *EMBO J.* **29**, 3358–3369

21. Budd, M. E., and Campbell, J. L. (1995) A new yeast gene required for DNA replication encodes a protein with homology to DNA helicases. *Proc. Natl. Acad. Sci. U. S. A.* **92**, 7642–7646

22. Budd, M. E., Choe, W. C., and Campbell, J. L. (2000) The nuclease activity of the yeast DNA2 protein, which is related to the RecB-like nucleases, is essential *in vivo*. *J. Biol. Chem.* **275**, 16518–16529

23. Jia, P. P., Junaid, M., Ma, Y. B., Ahmad, F., Jia, Y. F., Li, W. G., and Pei, D. S. (2017) Role of human DNA2 (hDNA2) as a potential target for cancer and other diseases: A systematic review. *DNA Repair (Amst.)* **59**, 9–19

24. Kumar, S., Peng, X., Daley, J., Yang, L., Shen, J., Nguyen, N., Bae, G., Niu, H., Peng, Y., Hsieh, H. J., Wang, L., Rao, C., Stephan, C. C., Sung, P., Ira,

G., *et al.* (2017) Inhibition of DNA2 nuclease as a therapeutic strategy targeting replication stress in cancer cells. *Oncogenesis* **6**, e319

25. Bae, S. H., Bae, K. H., Kim, J. A., and Seo, Y. S. (2001) RPA governs endonuclease switching during processing of Okazaki fragments in eukaryotes. *Nature* **412**, 456–461

26. Budd, M. E., Reis, C. C., Smith, S., Myung, K., and Campbell, J. L. (2006) Evidence suggesting that Pif1 helicase functions in DNA replication with the Dna2 helicase/nuclease and DNA polymerase delta. *Mol. Cell. Biol.* **26**, 2490–2500

27. Gobbini, E., Villa, M., Gnugnoli, M., Menin, L., Clerici, M., and Longhese, M. P. (2015) Sae2 function at DNA double-strand breaks is bypassed by dampening Tel1 or Rad53 activity. *PLoS Genet.* **11**, e1005685

28. Yu, T. Y., Kimble, M. T., and Symington, L. S. (2018) Sae2 antagonizes Rad9 accumulation at DNA double-strand breaks to attenuate checkpoint signaling and facilitate end resection. *Proc. Natl. Acad. Sci. U. S. A.* **115**, E11961–E11969

29. Arora, S., Deshpande, R. A., Budd, M., Campbell, J., Revere, A., Zhang, X., Schmidt, K. H., and Paull, T. T. (2017) Genetic separation of Sae2 nuclease activity from Mre11 nuclease functions in budding yeast. *Mol. Cell. Biol.* **37**, e00156-17

30. Budd, M. E., and Campbell, J. L. (2009) Interplay of Mre11 nuclease with Dna2 plus Sgs1 in Rad51-dependent recombinational repair. *PLoS One* **4**, e4267

31. Bae, S. H., Choi, E., Lee, K. H., Park, J. S., Lee, S. H., and Seo, Y. S. (1998) Dna2 of *Saccharomyces cerevisiae* possesses a single-stranded DNA-specific endonuclease activity that is able to act on double-stranded DNA in the presence of ATP. *J. Biol. Chem.* **273**, 26880–26890

32. Budd, M. E., and Campbell, J. L. (2000) The pattern of sensitivity of yeast dna2 mutants to DNA damaging agents suggests a role in DSB and postreplication repair pathways. *Mutat. Res.* **459**, 173–186

33. Hoa, N. N., Kobayashi, J., Omura, M., Hirakawa, M., Yang, S. H., Komatsu, K., Paull, T. T., Takeda, S., and Sasanuma, H. (2015) BRCA1 and CtIP are both required to recruit Dna2 at double-strand breaks in homologous recombination. *PLoS One* **10**, e0124495

34. Daley, J. M., Jimenez-Sainz, J., Wang, W., Miller, A. S., Xue, X., Nguyen, K. A., Jensen, R. B., and Sung, P. (2017) Enhancement of BLM-DNA2-mediated long-range DNA end resection by CtIP. *Cell Rep.* **21**, 324–332

35. Ceppi, I., Howard, S. M., Kasaciunaite, K., Pinto, C., Anand, R., Seidel, R., and Cejka, P. (2020) CtIP promotes the motor activity of DNA2 to accelerate long-range DNA end resection. *Proc. Natl. Acad. Sci. U. S. A.* **117**, 8859–8869

36. Ferrari, M., Dibitetto, D., De Gregorio, G., Eapen, V. V., Rawal, C. C., Lazzaro, F., Tsabar, M., Marini, F., Haber, J. E., and Pellicioli, A. (2015) Functional interplay between the 53BP1-ortholog Rad9 and the Mre11 complex regulates resection, end-tethering and repair of a double-strand break. *PLoS Genet.* **11**, e1004928

37. Öz, R., Howard, S. M., Sharma, R., Törnkvist, H., Ceppi, I., Kk, S., Kristiansson, E., Cejka, P., and Westerlund, F. (2020) Phosphorylated CtIP bridges DNA to promote annealing of broken ends. *Proc. Natl. Acad. Sci. U. S. A.* **117**, 21403–21412

38. Andres, S. N., Li, Z. M., Erie, D. A., and Williams, R. S. (2019) Ctp1 protein-DNA filaments promote DNA bridging and DNA double-strand break repair. *J. Biol. Chem.* **294**, 3312–3320

39. Carter, S. D., Vigasová, D., Chen, J., Chovanec, M., and Aström, S. U. (2009) Nej1 recruits the Srs2 helicase to DNA double-strand breaks and supports repair by a single-strand annealing-like mechanism. *Proc. Natl. Acad. Sci. U. S. A.* **106**, 12037–12042

40. Deshpande, R. A., and Wilson, T. E. (2007) Modes of interaction among yeast Nej1, Lif1 and Dnl4 proteins and comparison to human XLF, XRCC4 and Lig4. *DNA Repair (Amst.)* **6**, 1507–1516

41. Bustard, D., Menolfi, D., Jeppsson, K., Ball, L. G., Dewey, S. C., Shirahige, K., Sjögren, C., Branzei, D., and Cobb, J. A. (2012) During replication stress non-SMC-element 5 is required for Smc5/6 complex functionality at stalled forks. *J. Biol. Chem.* **287**, 11374–11383

42. Cannavo, E., Johnson, D., Andres, S. N., Kissling, V. M., Reinert, J. K., Garcia, V., Erie, D. A., Hess, D., Thomä, N. H., Enchev, R. I., Peter, M., Williams, R. S., Neale, M. J., and Cejka, P. (2018) Regulatory control of DNA end resection by Sae2 phosphorylation. *Nat. Commun.* **9**, 4016

43. Hohl, M., Mojumdar, A., Hailemariam, S., Kuryavyi, V., Ghisays, F., Sorenson, K., Chang, M., Taylor, B. S., Patel, D. J., Burgers, P. M., Cobb, J. A., and Petrini, J. H. J. (2020) Modeling cancer genomic data in yeast reveals selection against ATM function during tumorigenesis. *PLoS Genet.* **16**, e1008422

44. Bressan, D. A., Olivares, H. A., Nelms, B. E., and Petrini, J. H. (1998) Alteration of N-terminal phosphoesterase signature motifs inactivates *Saccharomyces cerevisiae* Mre11. *Genetics* **150**, 591–600

45. Foster, S. S., Balestrini, A., and Petrini, J. H. (2011) Functional interplay of the Mre11 nuclease and Ku in the response to replication-associated DNA damage. *Mol. Cell. Biol.* **31**, 4379–4389

46. Kim, H. S., Vijayakumar, S., Reger, M., Harrison, J. C., Haber, J. E., Weil, C., and Petrini, J. H. (2008) Functional interactions between Sae2 and the Mre11 complex. *Genetics* **178**, 711–723

47. Fu, Q., Chow, J., Bernstein, K. A., Makharashvili, N., Arora, S., Lee, C. F., Person, M. D., Rothstein, R., and Paull, T. T. (2014) Phosphorylation-regulated transitions in an oligomeric state control the activity of the Sae2 DNA repair enzyme. *Mol. Cell. Biol.* **34**, 778–793

48. Lobachev, K., Vitriol, E., Stemple, J., Resnick, M. A., and Bloom, K. (2004) Chromosome fragmentation after induction of a double-strand break is an active process prevented by the RMX repair complex. *Curr. Biol.* **14**, 2107–2112

49. Bonetti, D., Villa, M., Gobbini, E., Cassani, C., Tedeschi, G., and Longhese, M. P. (2015) Escape of Sgs1 from Rad9 inhibition reduces the requirement for Sae2 and functional MRX in DNA end resection. *EMBO Rep.* **16**, 351–361

50. Kumar, S., and Burgers, P. M. (2013) Lagging strand maturation factor Dna2 is a component of the replication checkpoint initiation machinery. *Genes Dev.* **27**, 313–321

51. Gilles, J. F., Dos Santos, M., Boudier, T., Bolte, S., and Heck, N. (2017) DiAna, an ImageJ tool for object-based 3D co-localization and distance analysis. *Methods* **115**, 55–64